Computational and Mathematical Methods in Medicine
Vol. 9, Nos. 3–4, September–December 2008, 327–337

Taylor & Francis
Taylor & Francis Group

Conformational changes in the connector protein complex of the bacteriophage ϕ29 DNA packaging motor

Arron C. Tolley and Nicola J. Stonehouse*

Astbury Centre for Structural Molecular Biology and Faculty of Biological Sciences, University of Leeds, Leeds, UK

(*Received 4 February 2008; final version received 29 March 2008*)

DNA packaging in the bacteriophage ϕ29 involves a molecular motor. It is proposed that dsDNA is packaged through a channel in a connector located at the 5-fold vertex of a preformed prolate icosahedral capsid. The packaging motor also consists of virally-encoded RNA molecules (pRNA) coupled to ATPases. Data obtained from studies using surface plasmon resonance, fluorescence quenching and circular dichroism are presented to demonstrate the importance of the N-termini of the connector protein subunits in pRNA interaction and in conformational change. Based on our findings, we propose a model of DNA packaging based on connector conformational change.

Keywords: RNA–protein interaction; bacteriophage ϕ29; molecular motor; virus assembly; conformational change

1. Introduction

Viruses have been identified in a wide range of organisms and all utilize a protein shell or capsid for the protection of their nucleic acid genome. The genome packaging event is therefore a key step in the lifecycle of every virus. In order to understand how these processes occur, it is important to dissect the fine details of the assembly pathway and characterize intermediates formed during nucleic acid packaging. Furthermore, an understanding of the molecular interactions involved may ultimately aid the design of novel therapeutics that target the formation of the assembly intermediates, thereby inhibiting production of infectious virus.

The bacteriophage ϕ29 is an ideal model system for the study of packaging events in dsDNA viruses. This relatively simple virus accomplishes genome packaging using a molecular motor. It is proposed that dsDNA is packaged through a channel located at the 5-fold vertex of a preformed prolate icosahedral capsid. The channel is composed of a complex of proteins (gp10) and is termed the portal or connector. The packaging motor also consists of virally-encoded RNA molecules (pRNA) coupled to ATPases, Figure 1(A). It has been reported that the ATPase molecules act in a sequential fashion, with each ATP hydrolysis event resulting in the translocation of 2 bp of DNA [4,8,13].

The crystal structure of the connector revealed a toroidal, dodecameric ring of gp10 proteins [5,20]; however, there is no high-resolution structure of the pRNA. This RNA is a highly structured 120 nt molecule which, in the presence of magnesium ions, has the ability to form multimeric structures via inter-molecular base pairing of complementary unpaired regions (Figure 1(B); [3,16]). The presence of pRNA monomers, dimers and trimers has been

*Corresponding author. Email: n.j.stonehouse@leeds.ac.uk

ISSN 1748-670X print/ISSN 1748-6718 online

DOI: 10.1080/17486700802168486
http://www.informaworld.com

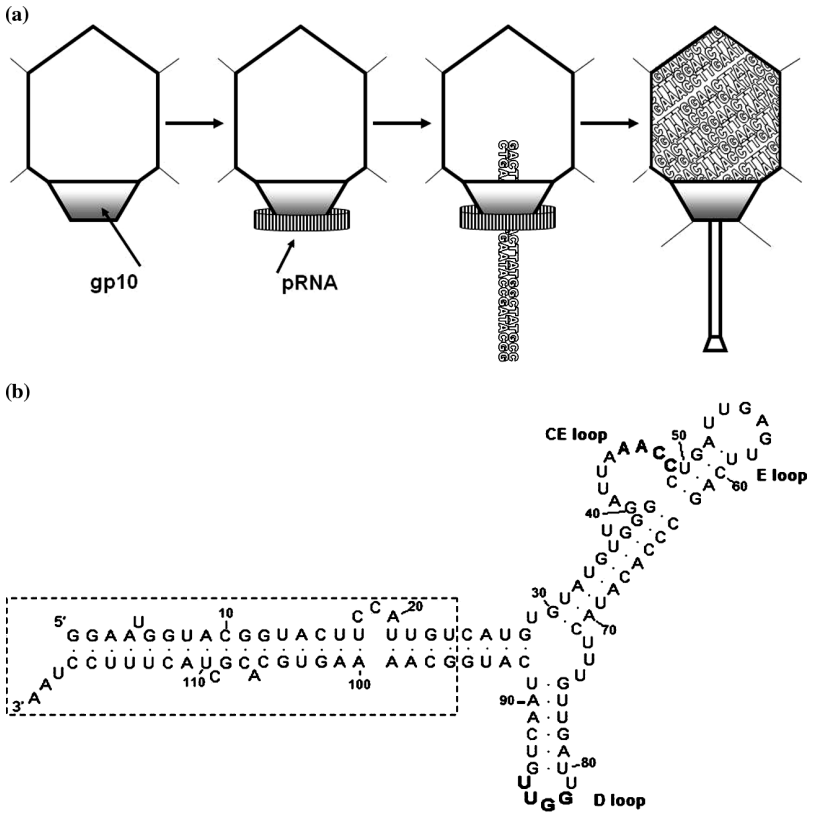

Figure 1. (A) Schematic representation of the components of bacteriophage ϕ29 during packaging of genomic dsDNA into the preformed capsid. The approximate locations of the connector and pRNA are shown. (B) The predicted secondary structure of ϕ29 120pRNA, as calculated by MFold [27]. Complementary bases in the CE and D loops implicated in pRNA multimerisation are in bold. Truncation of this molecule (removal of the boxed region) resulted in 71pRNA (with identical loop structure to 120pRNA). A mutant version, termed 71F6pRNA, incorporated mutations to remove complementarity between the CE and D loops [17,24]).

demonstrated in solution; however, it is thought that higher-order pRNA structures are present in the motor [24]. Both pentameric and hexameric pRNA rings have been proposed, with evidence for both [9,11,19,20,26]. Cryo-electron microscopy (cryo-EM) reconstruction of assembling ϕ29 particles revealed putative density for pRNA at the narrow end of the connector [22], indicating this region as the site of motor assembly and studies in Peixuan Guo's laboratory have shown that truncation of the N-terminal 14 amino acids of gp10 had deleterious effects on interaction with pRNA [25].

There have been several models proposed to explain how the motor functions. One model proposed that rotation of the pRNA about the connector caused linear translocation of the dsDNA genome [20]. However, previous studies in our laboratory have demonstrated a relatively high affinity between the connector and pRNA, suggesting that rotation between these components would be energetically unfavourable [17]. It was also shown that pRNA:connector binding affinity was increased in the presence of $MgCl_2$, even for mutant pRNA species that could not multimerize, indicating that $MgCl_2$-induced conformational changes may be involved in the pRNA:connector interaction [17]. Recent single molecule

studies have also shown that a rotation model of DNA packaging is unlikely, as no evidence of rotation of the connector was observed [10]. An alternative model, involving compression of the connector in a passive rotation ratchet-based mechanism, was suggested previously [4,18] and in the recent single molecule study a variation of this was proposed [10]. It was suggested that the spring-like shape of the connector could be important in packaging. Moreover, it was proposed that connector could undergo compression and expansion events, behaving like a 'chinese finger-trap' in order to prevent back-slippage of the DNA, thus, ensuring unidirectional packaging. The authors also suggested that conformational changes occurred in the ATPase component of the motor [2,10]; however, no direct experimental evidence has been produced to support these hypotheses.

Here, we report data obtained from studies using surface plasmon resonance (SPR), fluorescence quenching and circular dichroism (CD) to demonstrate the importance of the N-termini of the connector protein subunits in pRNA interaction and in conformational change in the connector itself. The data from SPR studies demonstrate the high affinity between the protein and pRNA components of the motor with the functional 120 nt pRNA molecule, as well as with a truncated version and with mutant pRNA (which can not multimerize). In addition, SPR provides further evidence that the pRNA binding site is on or near to the N-termini of the connector subunits. The changes in the CD spectra observed are indicative of divalent metal ion-induced conformational changes in the connector, which are ablated in the presence of an N-terminal histidine tag. We also report conformational changes in the connector that are induced by pRNA and propose a model of DNA packaging based on connector conformational change.

2. Materials and methods

2.1 Purification of connector proteins

C-terminally hexa-histidine-tagged gp10 connector protein (C-his connector) was purified by nickel-nitrilotriacetic acid (Ni-NTA) chromatography [17] followed by further purification with a HiTrap heparin column (G.E. Healthcare) in 10 mM Tris–HCl pH 7.6, 100 mM NaCl and elution in a NaCl gradient. In order to produce protein with an cleavable N-terminal tag (N-his connector), the gp10 gene was subcloned into pET-21(a) + (Novagen), downstream of a segment encoding a TEV protease cleavage site. Purification of N-his connectors was undertaken as above. In order to produce untagged connectors, samples of N-his connector in TEV dialysis buffer; 50 mM Tris–HCl, 0.5 mM EDTA (pH 8.0) were incubated in TEV cleavage buffer; 0.1 M DTT, 10 U TEV protease, 1 × TEV buffer, at 4°C for 2–3 days. Cleavage was monitored by SDS-PAGE. Mass spectrometry revealed the presence of an additional N-terminal glycine residue on the untagged protein, as expected. Transmission electron microscopy of all connector samples (negatively stained in uranyl acetate, 4%) was used to demonstrate the presence of discrete connector particles [17,21].

2.2 Synthesis of pRNA oligonucleotides

120pRNA is a shortened wild-type sequence that maintains the ability to multimerize and a DNA packaging activity equivalent to that of the wild type 174 nt pRNA [7]. 71pRNA represents bases 25–95 of 120pRNA, maintaining the potential to form inter-molecular base pairs and bind to the viral prohead [16]. 71F6pRNA is a derivative of 71pRNA with mutations in bases 45–48 of the CE loop, which prevent multimerization [17,24]. These three pRNA oligonucleotides (Figure 1(B)) were transcribed as described previously [17].

2.3 Surface plasmon resonance

N-his and C-his connectors were immobilized on separate flow cells on a Ni-NTA sensorchip surface (Biacore, Rapsgatan, Sweden). Approximately, 1800 response units (RU) of protein (where 1RU represents $1\,ng\,mm^{-2}$ protein) were immobilized in a continuous flow of fluorescence buffer; 50 mM Tris–HCl pH 7.6, 300 mM NaCl, 5% (v/v) glycerol, maintained at $20\,\mu l\,min^{-1}$ and at 21°C. Interactions between protein and pRNA were investigated in SPR running buffer; 10 mM HEPES pH 7.4, 150 mM NaCl, 0.005% (v/v) P20. 150 μl samples of pRNA oligonucleotides (at 10, 25, 100 and 200 nM) were injected (using the KINJECT function) for 450 s, followed by a 900 s wash. Subtraction of the sensorgram of an underivitized surface was used to remove any bulk refractive index changes due to the buffers. Data were analysed using the BiaEval software (Biacore). Equilibrium and kinetic binding constants were calculated by fitting the data to a 1:1 Langmuir association binding model, with χ^2 and residual values used to assess the quality of the fit. This model makes the assumption that the pRNAs are monomeric, as shown previously for the mutant 71F6pRNA by dynamic light scattering [17]. While at 5–8°C, multimerization-competent pRNAs existed in monomer-dimer-trimer equilibrium, at the elevated temperatures used here (~21°C) these pRNAs were predominantly monomeric [17,23].

2.4 Acrylamide fluorescence quenching

Fluorescence measurements were made on a FluroMax-3 (HORIBA Jobin Yvon Inc., Edison, NJ, USA) spectrofluorimeter. The excitation wavelength was set to 295 nm to limit excitation to tryptophan residues only. Emission spectra were recorded between 310 and 400 nm with 5 nm excitation and emission bandwidths. Samples of untagged connector in fluorescence buffer (0.075 μM) were analysed under four different experimental conditions: Connector alone; connector + 10 mM $MgCl_2$; connector + 0.9 μM 120pRNA; connector + 10 mM $MgCl_2$ and 0.9μM 120pRNA. Seven samples of each were prepared in the presence of increasing concentrations of acrylamide (up to 300 mM) and equilibrated at 21°C for 5 min before measurements were taken. Spectra were corrected for dilution and appropriate buffer scans subtracted from each. Stern–Volmer plots of the data were produced according to the relationship: $F_{tot}/F_0 = 1 + K_{SV}[Q]$, where F_{tot} is initial, total fluorescence (taken from the area under the curve of the connector-alone spectrum), F_0 is fluorescence at a given acrylamide concentration, K_{SV} is the Stern–Volmer quenching constant and Q is the concentration (in M) of quencher.

2.5 Circular dichroism

CD spectra were collected on a Jasco-715 spectrapolarimeter with a peltier temperature control unit set at 21°C. Samples of connector at $0.142\,mg\,ml^{-1}$ in CD buffer; 10 mM Tris-H_2SO_4 pH 7.6, 166 mM Na_2SO_4, or at $0.1\,mg\,ml^{-1}$ in fluorescence buffer (without glycerol) were examined in a 1 mm light path quartz cuvette (Helma UK, Ltd, Southend on Sea, Essex). Spectra and baseline data were taken in triplicate for each sample, collected between 180 and 260 nm at a resolution of 1 nm, bandwidth of 1 nm, sensitivity at 50 mdeg, five accumulations and a scan speed of $50\,nm\,min^{-1}$. Overlay plots showed the data to be virtually super-imposable; therefore the average values were taken. For accurate analysis, any data where the high tension measurements were found outside of the linear range during spectra acquisition were discarded. As a result, only data between 200 and 260 nm were used for analysis.

3. Results and discussion

3.1 Investigation of the roles of N- or C-terminal histidine tags on connector: pRNA interaction

Previous cryo-EM studies have indicated that the binding site for pRNA lies at the narrow end of the connector dodecamer [22]. Although, the N- and C-termini of the connector subunits are not observed in the crystal structure, it is likely that the N-termini of the gp10 subunits are in this region, with the C-termini closer to the wider end of the toroidal ring [20]. In order to investigate which region of the connector was required for pRNA interaction, the effect of the orientation of the connector on pRNA binding was probed by SPR. Samples of C- and N-terminally his-tagged connector (termed C-his and N-his, respectively) were immobilized on a Ni-NTA sensorchip and probed for RNA binding. Samples of pRNA oligonucleotides (at 10, 50, 100 and 200 nM) were injected over the sensorchip surface, allowing the interaction with the connector to be monitored in real time. It can be seen that 120pRNA interacted with the C-his connector in a concentration-dependent manor (Figure 2). Conversely, no such interaction was detectable between pRNA and the N-his connector. The same trends were also observed with the truncated 71pRNA and with the non-multimerizing 71F6pRNA (data not shown). It is therefore likely that the presence of the hexa-histidine tag or the orientation of the N-his connector on the sensorchip precluded binding of the pRNA. Sensorgrams were fitted to a 1:1 (Langmuir) association model, as described in the Materials and Methods section. The quality of these fits is shown by the χ^2 values (Table 1). Although, it is unlikely that the multimerization-incompetent 71F6pRNA will bind cooperatively, the possibility of cooperative binding for the other pRNA oligonucleotides cannot be ruled out; however, all of the data fit well to a 1:1 model. The K_D values obtained were all in the low nM range (and similar within experimental error) at 1.88, 22.1 and 4.9 nM for 120pRNA, 71pRNA and 71F6pRNA, respectively. These values are up to 200-fold lower than the K_{Dapp} values, we reported previously [17]. These values were derived from bead-based binding assays which

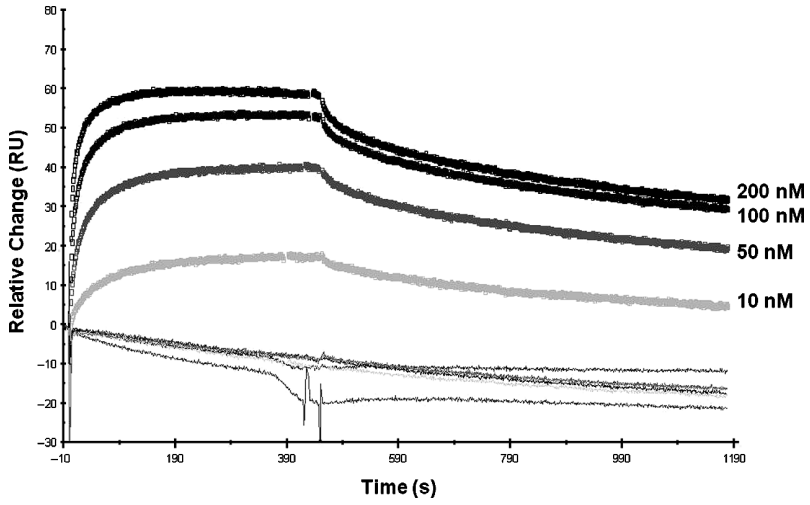

Figure 2. SPR sensorgram of the interaction between connector and pRNA. 120pRNA (10, 50, 100 and 200 nM) was injected over flow cells immobilized with either C-his or N-his connector. Interaction with C-his connector (thick lines) shows clear association, equilibrium and dissociation phases. Conversely, immobilized N-his connector (thin lines) did not show any significant interaction with the pRNA.

Table 1. Shows the calculated association and dissociation rate constants obtained during real-time SPR studies.

RNA	*k*a 1/M/s	*k*d 1/s	K_d M
120pRNA	4.79^{5}	9.03^{-4}	1.89^{-9}
71pRNA	3.05^{5}	6.74^{-3}	2.21^{-8}
71F6pRNA	6.67^{5}	3.30^{-3}	4.95^{-9}
	χ^2	χ^2	Average χ^2
120pRNA	0.199	0.116	0.158
71pRNA	0.085	0.09	0.74
71F6pRNA	0.054	0.066	0.06

The χ^2 values are a statistical representation of the closeness of the fit of the data to the theoretical 1:1 Langmuir binding model.

rely on the physical separation of equilibrium mixtures and can result in over-estimations of K_D values. Based on the data reported here, we propose that the pRNA:connector interaction is of even higher affinity than previously estimated.

3.2 Quenching of intrinsic tryptophan fluorescence suggests a conformational change in the connector

Many models of bacteriophage DNA packaging involve rotation of one or more motor components [6,12,20]. However, there is no experimental evidence to support a rotation model for ϕ29 and recent investigations have shown this to be improbable [10]. The high affinity interaction between the pRNA and the connector also makes relative rotation between these components unlikely. An alternative model could involve conformational changes in one or

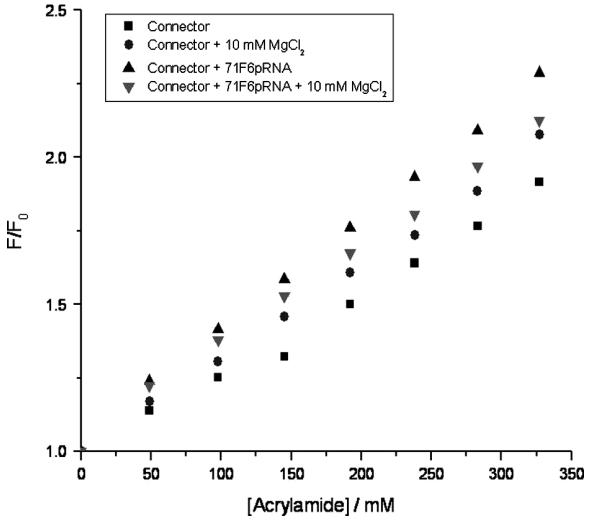

Figure 3. Stern–Volmer plot of the acrylamide quenching of intrinsic tryptophan fluorescence of untagged connector with $MgCl_2$ and 71F6pRNA, according to the relationship: $F_{tot}/F_0 = 1 + K_{SV}[Q]$, where F_{tot} is initial native fluorescence, F_0 is fluorescence intensity at a given acrylamide concentration, K_{SV} is the collisional quenching constant and Q is the concentration of quencher. The increases in K_{SV} are suggestive of conformational change in the protein in the presence of $MgCl_2$ and pRNA.

more components of the motor and we have previously proposed that such changes in pRNA may be important in motor function [17]. However, no experimental evidence of connector conformational changes has been reported.

In order to probe conformational change in the connector, the effect of acrylamide on the fluorescence intensity was measured under different experimental conditions. Each connector subunit contains three tryptophan residues, located at least 40 Å from the putative pRNA binding site [20]. These contribute to the intrinsic fluorescence of the protein. Any changes in the local environment of these amino acids can cause a shift in λ_{max} or a change in the fluorescence intensity. Untagged connectors were used for these experiments and the change in intrinsic tryptophan fluorescence was measured (with increasing concentrations of acrylamide) in the presence and absence of non-multimerizing 71F6pRNA, 10 mM $MgCl_2$ or both. Stern–Volmer plots (Figure 3) show there is increased quenching of the connector tryptophan residues in the presence of 10 mM $MgCl_2$. This is indicative of a change in local environment, with one or more of the tryptophans further exposed, reflected by increase in the Stern–Volmer equilibrium constant (K_{SV}) from 2.6 to 3.2. This effect is enhanced in the presence of pRNA ($K_{SV} = 3.7$), although pRNA alone seemed to have the greatest effect ($K_{SV} = 4.2$). Although, relatively modest, these increases in K_{SV} are representative of an increased frequency of collisions between the quencher and the fluorophore. As the trypotophans are located distally to the putative pRNA binding site (at the narrow end of the connector) these data are suggestive of both pRNA- and $MgCl_2$-induced conformational changes in the connector.

3.3 Probing divalent metal ion and pRNA induced conformational changes in the connector by circular dichroism spectroscopy

CD spectroscopy provides a means for detecting changes in the secondary and tertiary structure of proteins. Three variants of the connector (C-his, N-his and untagged) were used to probe such conformational changes in the presence and absence of $MgCl_2$. The CD spectra shown in Figure 4, demonstrate the α-helical nature of this protein, as expected from the crystal structure [20] and suggest that both the C-his connector and untagged connector became less α-helical in the presence of 10 mM $MgCl_2$ (Figure 4(A) and (B)). In contrast, the structure of the N-his connector was not affected by the presence of $MgCl_2$ (Figure 4(C)). The data therefore suggest that conformational changes are occurring which may be obstructed by the presence of the N-terminal hexa-histidine tag, consistent with conformational changes in or around the N-terminus of the connector. This is consistent with the reduced pRNA oligonucleotide binding described above. In order to investigate whether this was magnesium ion–dependent or driven by other divalent metal cations, the experiment was repeated with 10 mM $MgSO_4$ or $MnCl_2$. Both were equally effective in generating conformational changes in the protein (data not shown). We therefore suggest that the conformational change in the connector is probably driven by divalent metal ion interaction and not specifically magnesium ions.

In order to investigate the influence of pRNA binding on connector structure, the effect of non-multimerizing 71F6pRNA on the structure of untagged connector was measured (in the presence and absence of 10 mM $MgCl_2$). Although RNA can have a significant CD signal in the far UV spectrum, under the experimental conditions used pRNA alone did not contribute significantly to the spectrum (Figure 5). However, the presence of pRNA did have a clear effect on the spectrum of the connector and this effect was greatly enhanced in the presence of $MgCl_2$. Spectra taken over a 10 min period were virtually super-imposable, therefore these effects are unlikely to be the result of aggregation or dissociation of the connector. Spectra at lower protein concentrations (*i.e.* less than 0.12 mg ml^{-1}) were often more variable between experiments;

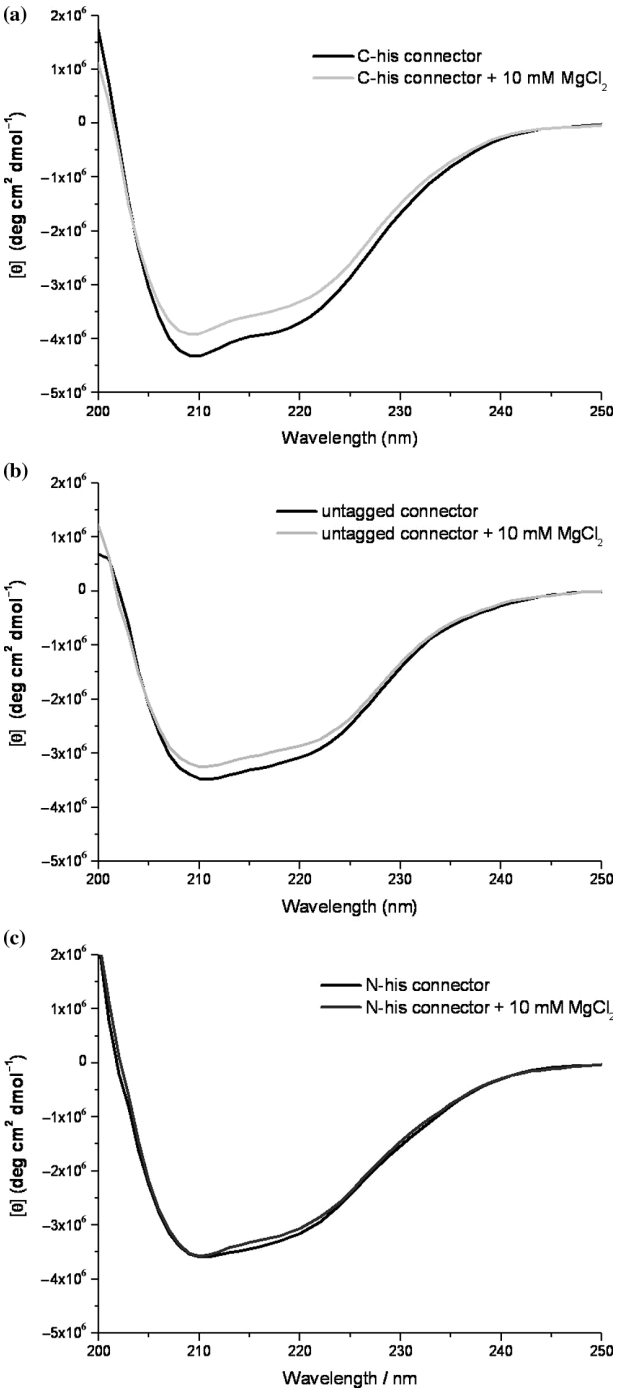

Figure 4. CD spectra of connectors (0.142 mg ml^{-1} in 10 mM Tris-H_2SO_4 pH 7.6, 166 mM Na_2SO_4) in the presence and absence of $MgCl_2$. C-his and untagged connectors (panels (A) and (B), black) show a decrease in signal in the presence of $MgCl_2$ (grey), consistent with conformational change. (C) Little change is seen with N-his connectors.

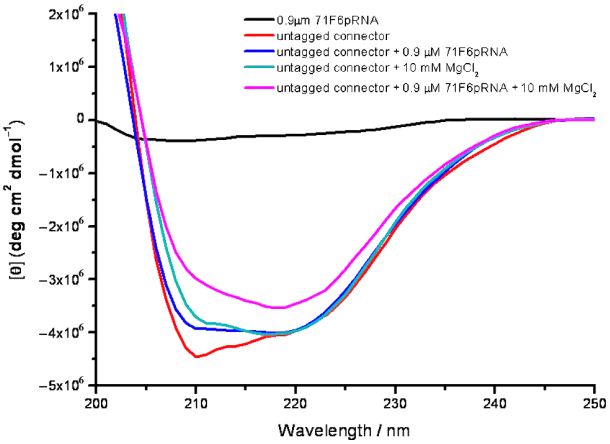

Figure 5. CD spectra of untagged connectors (0.1 mg ml^{-1} in 50 mM Tris–HCl pH 7.6, 300 mM NaCl) in the presence and absence of $MgCl_2$ and 71F6pRNA. pRNA (0.9 µM) contributes very little to the spectra (black). In addition to a bathochromic shift from 208 to 210 nm, there is a hypochromic shift in the 210 nm range when $MgCl_2$ (green) or pRNA were added (blue). However, the greatest effect was observed when both were present (pink), consistent with a change in conformation of the protein induced by pRNA and by $MgCl_2$ under these conditions.

however, the trends seen were consistent. We therefore feel that these changes are indicative of a pRNA-mediated conformational change in connector over that of divalent metal ions alone.

3.4 In conclusion

Our data are in agreement with previously published work [22,25] suggesting that pRNA binds adjacent to the N-termini of connector subunits. In addition, we have extended our previous studies on pRNA-connector affinity and obtained the first real-time measurements of the affinity between these two components of the motor. We have also obtained the first evidence of conformational change in the connector complex and shown that the N-terminal region of the connector is likely to be the site of this change. The flexibility of the narrow end of the connector has been demonstrated previously by atomic force microscopy [15]. It was shown that this part of the molecule was reversibly compressible, although it was not clear if this observation was functionally significant. Our data clearly show that conformational changes in the ϕ29 connector occur in the presence of $MgCl_2$, and that there is an additional effect in the presence of pRNA. Non-multimerizing 71F6pRNA was used for these studies; however, it is clear that multimerization is important for motor function [9,16]. We suggest that multimerization competency may play an important role in modulating the extent of the conformational changes seen in the connector. This hypothesis will be tested with the use of multimerization-competent pRNAs in future studies. It is interesting to note that the portal of the bacteriophage P22 has also been demonstrated to contain a flexible N-terminal region [14] and that $MgCl_2$-induced conformational changes have been shown to be important in structural stability of the polymerase enzyme from hepatitis C virus, due to exposure of hydrophobic residues [1].

It is clear from our studies that the high affinity between motor components would make rotation of the pRNA about the connector energetically unfavourable. Indeed, there is no evidence in the literature to support a model based on rotation. However, we have shown that the

connector can undergo conformational changes, modulated by pRNA and by divalent metal ions. We therefore propose that conformational changes in the connector drive the packaging of the dsDNA. It is possible that metal ion-binding is required to stabilize the optimal conformation of the connector for interaction with pRNA. It is also interesting to note that magnesium ions are required for hydrolysis of ATP by the motor component gp16. It is tempting to speculate that cycles of sequestration and release of intracellular could be used to modulate ATPase activity *in vivo*.

Acknowledgements

We would like to thank BBSRC (UK) for funding (0340 and 24/C17944), Stephanie Capaldi for the cloning of N-his gp10 and Alison Ashcroft for mass spectrometry.

References

[1] I. Benzaghou, I. Bougie, and M. Bisaillon, *Effect of metal ion binding on the structural stability of the hepatitis C virus RNA polymerase*, J. Biol. Chem. 279 (2004), pp. 49755–49761.
[2] Y.R. Chemla, K. Aathavan, J. Michaelis, S. Grimes, P.J. Jardine, D.L. Anderson, and C. Bustamante, *Mechanism of force generation of a viral DNA packaging motor*, Cell 122 (2005), pp. 683–692.
[3] C.P. Chen, S.T. Sheng, Z.F. Shao, and P.X. Guo, *A dimer as a building block in assembling RNA – a hexamer that gears bacterial virus ϕ29 DNA-translocating machinery*, J. Biol. Chem. 275 (2000), pp. 17510–17516.
[4] S. Grimes, P.J. Jardine, and D. Anderson, *Bacteriophage phi 29 DNA packaging*, Adv. Virus Res. 58 (2002), pp. 255–294.
[5] A. Guasch, A. Parrága, J. Pous, J.M. Valpuesta, J.L. Carrascosa, and M. Coll, *Purification, crystallization and preliminary X-ray diffraction studies of the bacteriophage ϕ29 connector particle*, FEBS Lett. 430 (1998), pp. 283–287.
[6] A. Guasch, J. Pous, B. Ibarra, F.X. Gomis-Ruth, J.M. Valpuesta, N. Sousa, J.L. Carrascosa, and M. Coll, *Detailed architecture of a DNA translocating machine: The high- resolution structure of the bacteriophage phi 29 connector particle*, J. Mol. Biol. 315 (2002), pp. 663–676.
[7] P. Guo, S. Bailey, J.W. Bodley, and D. Anderson, *Characterization of the small RNA of the bacteriophage ϕ29 DNA packaging machine*, Nucleic Acids Res. 15 (1987), pp. 7081–7090.
[8] P. Guo and T.J. Lee, *Viral nanomotors for packaging of dsDNA and dsRNA*, Mol. Microbiol. 64 (2007), pp. 886–903.
[9] P. Guo, C. Zhang, C. Chen, K. Garver, and M. Trottier, *Inter-RNA interaction of phage ϕ29 pRNA to form a hexameric complex for viral DNA transportation*, Mol. Cell 2 (1998), pp. 149–155.
[10] T. Hugel, J. Michaelis, C.L. Hetherington, P.J. Jardine, S. Grimes, J.M. Walter, W. Falk, D.L. Anderson, and C. Bustamante, *Experimental test of connector rotation during DNA packaging into bacteriophage phi29 capsids*, PLoS Biol. 5 (2007), p. e59.
[11] B. Ibarra, J.R. Castón, O. Llorca, M. Valle, J.M. Valpuesta, and J.L. Carrascosa, *Topology of the components of the DNA packaging machinery in the phage ϕ29 prohead*, J. Mol. Biol. 298 (2000), pp. 807–815.
[12] A.A. Lebedev, M.H. Krause, A.L. Isidro, A.A. Vagin, E.V. Orlova, J. Turner, E.J. Dodson, P. Tavares, and A.A. Antson, *Structural framework for DNA translocation via the viral portal protein*, EMBO J. 26 (2007), pp. 1984–1994.
[13] C.-S. Lee and P. Guo, In vitro *assembly of infectious virions of double-stranded DNA phage ϕ29 from cloned gene products and synthetic nucleic acids*, J. Virol. 69 (1995), pp. 5018–5023.
[14] S.D. Moore and P.E. Prevelige, Jr., *Structural transformations accompanying the assembly of bacteriophage P22 portal protein rings* in vitro, J. Biol. Chem. 276 (2001), pp. 6779–6788.
[15] D.J. Muller, A. Engel, J.L. Carrascosa, and M. Velez, *The bacteriophage phi29 head-tail connector imaged at high resolution with the atomic force microscope in buffer solution*, EMBO J. 16 (1997), pp. 2547–2553.
[16] R. Reid, F. Zhang, S. Benson, and D. Anderson, *Probing the structure of bacteriophage ϕ29 prohead RNA with specific mutations*, J. Biol. Chem. 269 (1994), pp. 18656–18661.
[17] M.A. Robinson, J.P. Wood, S.A. Capaldi, A.J. Baron, C. Gell, D.A. Smith, and N.J. Stonehouse, *Affinity of molecular interactions in the bacteriophage phi29 DNA packaging motor*, Nucleic Acids Res. 34 (2006), pp. 2698–2709.

[18] P. Serwer, *Models of bacteriophage DNA packaging motors*, J. Struct. Biol. 141 (2003), pp. 179–188.
[19] D. Shu, H. Zhang, J. Jin, and P. Guo, *Counting of six pRNAs of phi29 DNA-packaging motor with customized single-molecule dual-view system*, EMBO J. 26 (2007), pp. 527–537.
[20] A.A. Simpson, Y.Z. Tao, P.G. Leiman, M.O. Badasso, Y.N. He, P.J. Jardine, N.H. Olson, M.C. Morais, S. Grimes, D.L. Anderson et al., *Structure of the bacteriophage ϕ29 DNA packaging motor*, Nature 408 (2000), pp. 745–750.
[21] N.J. Stonehouse and P.G. Stockley, *Effects of amino acid substitution on the thermal stability of MS2 capsids lacking genomic RNA*, FEBS Lett. 334 (1993), pp. 355–359.
[22] Y. Tao, N.H. Olson, W. Xu, D.L. Anderson, M.G. Rossmann, and T.S. Baker, *Assembly of a tailed bacterial virus and its genome release studied in three dimensions*, Cell 95 (1998), pp. 431–437.
[23] J.P.A. Wood, *Characterisation of the self-association of bacteriophage phi29 pRNA*, PhD Thesis, University of Leeds, 2002.
[24] J.P.A. Wood, S.A. Capaldi, M.A. Robinson, A.J. Baron, and N.J. Stonehouse, *RNA multimerisation in the DNA packaging motor of bacteriophage ϕ29*, J. Theor. Med. 6 (2005), pp. 127–134.
[25] F. Xiao, W.D. Moll, S. Guo, and P. Guo, *Binding of pRNA to the N-terminal 14 amino acids of connector protein of bacteriophage phi29*, Nucleic Acids Res. 33 (2005), pp. 2640–2649.
[26] F. Zhang, S. Lemieux, X.L. Wu, D. StArnaud, C.T. McMurray, F. Major, and D. Anderson, *Function of hexameric RNA in packaging of bacteriophage ϕ29 DNA* in vitro, Mol. Cell 2 (1998), pp. 141–147.
[27] M. Zuker, *Mfold web server for nucleic acid folding and hybridization prediction*, Nucleic Acids Res. 31 (2003), pp. 3406–3415.